minerals

MDPI

Article

Re-Os Isotope Systematics of Sulfides in Chromitites and Host Lherzolites of the Andaman Ophiolite, India

José María González-Jiménez [1,2,*], Sisir K. Mondal [3], Biswajit Ghosh [4], William L. Griffin [2] and Suzanne Y. O'Reilly [2]

1 Departamento de Mineralogía y Petrología, Facultad de Ciencias, Universidad de Granada, Avda. Fuentenueva s/n, 18002 Granada, Spain
2 Australian Research Council Centre of Excellence for Core to Crust Fluid Systems (CCFS) and GEMOC, Macquarie University, Sydney NSW 2109, Australia; bill.griffin@mq.edu.au (W.L.G.); sue.oreilly@mq.edu.au (S.Y.O.)
3 Department of Geological Sciences, Jadavpur University, 188, Raja SC Mullick Road, Kolkata, West Bengal 700032, India; sisir.mondal@gmail.com
4 Department of Geology, University of Calcutta, 35 Ballygunge Circular Road, Kolkata 700019, India; bghosh_geol@hotmail.com
* Correspondence: jmgonzj@ugr.es; Tel.: +34-958-246-619

Received: 2 July 2020; Accepted: 29 July 2020; Published: 31 July 2020

Abstract: Laser ablation MC-ICP-MS was used to measure the Os-isotope compositions of single sulfide grains, including laurite (RuS_2) and pentlandite [$(Fe,Ni)_9S_8$], from two chromitite bodies and host lherzolites from ophiolites of North Andaman (Indo-Burma-Sumatra subduction zone). The results show isotopic heterogeneity in both laurite (n = 24) and pentlandite (n = 37), similar to that observed in other chromitites and peridotites from the mantle sections of ophiolites. Rhenium-depletion model ages (T_{RD}) of laurite and pentlandite reveal episodes of mantle magmatism and/or metasomatism in the Andaman mantle predating the formation of the ophiolite (and the host chromitites), mainly at ≈0.5, 1.2, 1.8, 2.1 and 2.5 Ga. These ages match well with the main tectonothermal events that are documented in the continental crustal rocks of South India, suggesting that the Andaman mantle (or its protolith) had a volume of lithospheric mantle once underlaying this southern Indian continental crust. As observed in other oceanic lithospheres, blocks of ancient subcontinental lithospheric mantle (SCLM) could have contributed to the development of the subduction-related Andaman–Java volcanic arc. Major- and trace-element compositions of chromite indicate crystallization from melts akin to high-Mg IAT and boninites during the initial stages of development of this intra-oceanic subduction system.

Keywords: ophiolite; chromitite; platinum-group minerals; osmium isotopes; Andaman; subduction zone

1. Introduction

The association of chromitites with dunite diking harzburgite, and to a lesser extent lherzolite, of the mantle section of ophiolite complexes is well known [1–3]. Differences in the assemblages of mineral inclusions found in the chromitite have led to a profusion of models to explain their formation and evolution in the Earth's upper mantle [4–30]. Other studies have analyzed the Re-Os isotopic systematics of chromitites and host peridotites in order to understand the genetic processes of chromitites and host peridotites within the oceanic mantle [8,31–33]. The in situ analyses of Re-Os isotopic composition of platinum-group minerals (PGM) and base-metal sulfides (BMS) using of LA-MC-ICP-MS have revealed significant isotopic heterogeneities in Os at all scales (km, hand-specimen, thin sections and within single grain) in both chromitites and host peridotites in the upper mantle [32,34–42]. The high degree

of isotopic heterogeneity in the chromitite was interpreted as reflecting their formation from different pulses of melts that were extracted from mantle sources with a protracted history of partial melting and metasomatism. In fact, a comparison of rhenium-depletion model ages (T_{RD}) obtained for PGM and BMS from both chromitites and host peridotite with well-constrained independent geochronological data indicates that mantle melt depletion and refertilization recorded in mantle PGM and BMS are often linked to episodes of crustal growth [12,37,40,41], thus providing evidence that Re-Os isotopes in these minerals are a powerful tool for developing a full understanding of the complex geological evolution of oceanic lithospheres.

In this paper, we aim to contribute to the ongoing debate on chromitite genesis in the upper mantle and their potential application for constraining the evolution of oceanic lithosphere by using the first Re-Os data for PGM and BMS of chromitites and host peridotites from the North Andaman ophiolite. This is one of the unique examples of a fore-arc basin ophiolite in which chromitites are hosted in lherzolites. This gives us an unusual opportunity to evaluate the genesis and evolution of chromitites within the framework of a previously unrecognized geological scenario. Here, we analyzed major- and trace- elements of chromite from the Andaman chromitites by means of Electron-Probe Micro Analyzer EPMA and expand (LA-ICP-MS) as well as Re-Os isotopes in individual PGM and BMS found as inclusions in chromite of chromitite and from host lherzolite, respectively. The acquired data are integrated in order to outline a model for the formation of the chromitites to constrain the evolutionary history of the oceanic lithosphere related to the Andaman ophiolite.

2. Geological Background

The collisional boundary at the northern margin of the Indian plate along the E–W trending Himalayan Indus–Yarlung Tsangpo suture extends south from the eastern Himalayan syntaxis through Nagaland, Manipur and the western Burma (Myanmar) region and merges with modern Indonesian subduction system along the Andaman–Sumatra–Java (ASZ) trench where the Indian plate is pushing beneath the Myanmar sub-plate [43]. The Andaman and Nicobar Islands form the outer arc high (Figure 1a), constituting an accretionary prism composed of remnant Cretaceous ophiolites with underlying mélange and a Palaeogene–Neogene sedimentary succession [44,45].

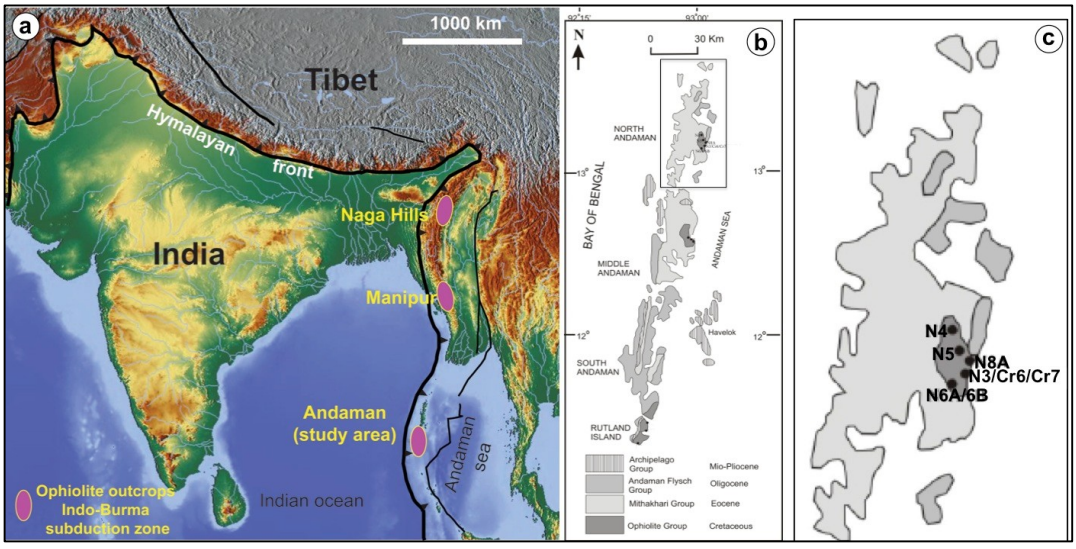

Figure 1. (**a**) Location of the Andaman and Nicobar Islands within the geological framework of the Indo-Burma-Sumatra subduction zone (Plate boundaries after [46]); (**b**,**c**) Schematic maps of North Andaman showing the location of the samples employed in this study at the north part of the Island.

Discontinuous occurrences of ophiolitic rocks crop out along the east coast of North, Middle, South Andaman and Rutland Islands (Figure 1b,c; [47–49]). An idealized coherent ophiolite stratigraphy is

nowhere exposed in the islands; instead various lithologies comprising a tectonized, variably fertile and restitic mantle sequence hosting chromitite pods, an intrusive crustal cumulate and volcanic sequences occur as dismembered units [45]. U–Pb zircon dating of the plagiogranites from South Andaman has dated the ophiolites at ≈95 Ma [50,51]. However, from the Ar/Ar dating of amphiboles from the metamorphic sole [52] define the age of ophiolite formation as ≈105 Ma.

In terms of petrography and mineral chemistry of the mantle peridotites, a pronounced variation exists between Rutland Island to the south and North Andaman to the north [53]. The mantle section on the Rutland Island is harzburgite-dominated, consistent with 14–18% hydrous mantle melting [43] in a suprasubduction zone environment [54]. In contrast, the ophiolites in north Andaman are dominated by relatively fertile lherzolites that occasionally grade to clinopyroxene-bearing harzburgites [44]. Small chromitite pods, semi-oval to lenticular in shape, are restricted within dunite melt channels diking the lherzolites [43,44]. Therefore, the podiform chromitites on north Andaman are atypical, being hosted in lherzolites [55], unlike most other global occurrences, which are associated with harzburgites [3,9].

3. Materials and Methods

3.1. Samples

The samples employed in this study were collected from two different chromitite pods known as Cr-6, Cr-7 and corresponding host lherzolite (N-3, N-4, N-5, N-6) North Andaman (Figure 1). Among these samples, the chromitite pods and one peridotite (N-3) were sampled from a quarry section. The remaining samples of peridotites were collected from the surface exposures near to the chromitite pods.

3.2. Chromite

The major element composition of chromite was determined on polished sections using a Cameca SX-100 microprobe in the Geochemical Analysis Unit at Australian Research Council Centre of Excellence for Core to Crust Fluid Systems (CCFS) and Key Centre for Geochemistry and Metallogeny of Continents (GEMOC), Macquarie University. The system is equipped with five wavelength dispersive spectrometers and a Princenton Gamma Tech energy dispersive system. The analyses were performed using 15 kV acceleration voltage, 20 nA sample current, and a beam size of ≈2 µm. The following counting times were employed: 10 s peak counting times for Ca, Cr, Fe, K, Mn, Na, Ni, Ti, V and Zn; 20 s for Mg and Si; and 30 s for Al. The counting times for background signals were half the peak counting times on each side of the respective peak. Standards used were a combination of natural and synthetic minerals and pure metals. Matrix corrections followed the method by [56]. Structural formulae of chromite were calculated assuming stoichiometry following the procedure of [57]. Representative electron-microprobe analyses of chromite are listed in Table S1.

The minor and trace element compositions of chromite were determined using a Wave UP 266 laser system connected to an Agilent 7500cs ICP-MS in the Geochemical Analysis Unit, CCFS/GEMOC. For this study, the chromite was analyzed for the following masses: ^{45}Sc, ^{47}Ti, ^{51}V, ^{55}Mn, ^{59}Co, ^{60}Ni, ^{66}Zn and ^{71}Ga. The analyses were conducted using a ~55 µm beam diameter, 5 Hz frequency, and 4.16 mJ/pulse power, during 180 s analysis (60 s for the gas blank and 120 s on the chromite). The data were processed using the GLITTER software [58]. The instrument was calibrated against the NIST 610 silicate glass (National Institute Standards and Technology, Gaithersburg, MD, USA) [59]. Aluminum values obtained by electron-microprobe were used as the internal standard to determine the minor and trace element concentrations. The basaltic glass BRC-2g [59,60] and the in-house standard LCR-1 (Lace mine, South Africa) were analysed as unknowns during each analytical chromite run to check for accuracy and precision of the analyses. The results obtained during the analyses of these two standards display very good reproducibility for most trace elements < 5%. Results of minor- and trace-element analysis for chromite are provided in Table S2.

The major-element composition of chromite obtained by electron-microprobe was used to calculate the parental melt composition of the chromitite. This estimate was obtained applying the series of algorithms mentioned below. The Al_2O_3 content of the melt from which chromite crystallized was computed using the equation proposed by [61]) (Equation (1)) and those implemented by [62] and [63] for arc melts (Equations (2) and (3), respectively), which were partially derived from [64]:

$$(Al_2O_3)_{spinel} = 0.035(Al_2O_3)^{2.42}{}_{melt} \quad (1)$$

$$(Al_2O_3)_{melt} = 5.2181 \cdot \ln (Al_2O_3)_{spinel} - 1.0505 \quad (2)$$

$$(Al_2O_3)_{melt} = 5.2253 \cdot \ln (Al_2O_3)_{spinel} - 1.1232 \quad (3)$$

The regression expression for chromite from arc settings used inasmuch as the chromites from the Andaman chromitites show compositions similar to chromites from arc lavas. The algorithm proposed by [64] and redesigned by [62] and [63] for arc-derived melts was also applied to calculate the TiO_2 content of the parental melt (Equations (4) and (5), respectively):

$$(TiO_2)_{melt} = 1.0963(TiO_2)^{0.7863}{}_{spinel} \quad (4)$$

$$(TiO_2)_{melt} = 1.0897(TiO_2)_{spinel} + 0.0892 \quad (5)$$

The FeO/MgO ratio of the melt in equilibrium with chromite was estimated using the empirical expression of [65]:

$$\ln(FeO/MgO)_{spinel} = 0.47 - 1.07Al\#_{spinel} + 0.64Fe^{3+}\#_{spinel} + \ln(FeO/MgO)_{melt} \quad (6)$$

with FeO and MgO in wt.%, $Al\#_{spinel} = Al/(Cr + Al + Fe^{3+})$ and $Fe^{3+}\#_{spinel} = Fe^{3+}/(Cr + Al + Fe^{3+})$.

3.3. Platinum-Group Minerals and Base-Metal Sulfides

Polished thin-sections of the chromitite samples were studied under the optical microscopy in reflected and transmitted light to characterize rock textures and detect platinum-group minerals (PGM) and base-metal sulfides (BMS). Once located, the PGM and BMS were then imaged and identified qualitatively by their characteristic Energy Dispersive Spectra (EDS) using a ZEISS EVO MA15 Scanning Electron Microscope (SEM) in the Geochemical Analysis Unit, CCFS/GEMOC, Sydney, Australia. Grains larger than 2 μm across were later analyzed using the Cameca SX-100 electron-microprobe, under the following operating conditions: accelerating voltage 20 kV, sample current 30 nA, and beam size ~2 μm. The X-ray lines measured were Kα for S, Fe, Co, Ni, Cu, Cr and As; Lα for Ru, Rh, Ir, Pt; Lβ for Pd and Mα for Os. Pure metals were used as standards for Os, Ir, Ru, Rh, Pt, Pd, Ni, Co; FeS_2 for Fe, $CuFeS_2$ for S and Cu; chromite for Cr and NiAs for As. Because of the small size of the particles, the raw data show moderate Cr concentrations due to excitation of the chromite matrix. These data were corrected, by subtraction of Cr and the corresponding proportion of Fe due to the host chromite (determined from its Cr/Fe ratio), and the atomic concentrations were calculated from the corrected analytical data. At least two analyses were performed on each large grain to check the homogeneity. Representative electron-microprobe analyses of PGM are listed in Table S3.

Grains of PGM > 5 μm and BMS ≥ 50 μm across were selected for in situ Re-Os isotope analysis in the Geochemical Analysis Unit at CCFS/GEMOC. A New Wave/Merchantek UP 213 laser microprobe with a modified ablation cell was coupled with a Nu Plasma Multicollector ICP-MS. During the runs for PGM analysis all ion beams were collected in Faraday cups. The laser was fired at a frequency of 4 Hz, with energies of 1–2 mJ/pulse and a spot size of 15 μm. During ablation runs, a standard NiS bead (PGE-A) with 199 ppm Os and $^{187}Os/^{188}Os = 0.1064$ was analyzed between samples to monitor any drift in the Faraday cups. These variations typically were less than 0.1% over a long day's analytical session. The overlap of ^{187}Re on ^{187}Os was corrected by measuring the ^{185}Re peak and

using $^{187}Re/^{185}Re = 1.6742$. All the analyzed grains had $^{187}Re/^{188}Os$ lower than 0.5, thus ensuring that the isobaric interference of ^{187}Re on ^{187}Os was precisely corrected (c.f. [66]). The data were collected using the Nu Plasma time-resolved software, which allows the selection of the most stable intervals of the signal for integration. The selected interval was divided into 40 replicates to provide a measure of the standard error. For PGM with grain sizes of 5 μm and Os contents > 1 wt.%, a typical run duration of ~75 s was achieved and signal intensity of Os > 0.2 volts was obtained in the Faraday cups, resulting a precision for $^{187}Os/^{188}Os$ ranging from 4.6×10^{-5} to 1.9×10^{-3} (2SE). The accuracy of the data presented here is illustrated by independent analyses (different instruments, operating protocols) of Os-Ir alloys from chromitites in the Luobusa (Tibet) ophiolite by [32]. They reported a mean $^{187}Os/^{188}Os = 0.12646 \pm 11$ (1SE, n = 148) that is identical to $^{187}Os/^{188}Os = 0.12653 \pm 7$ (1SE, n = 80) reported by [42]. Several tests were carried out to verify the low contents of Re and Os in the host chromite and silicates compared to the PGM. These tests showed that the partial inclusion of chromite or silicate in the ablated volume gave negligible contributions to the sampled Re and Os budgets.

During the runs for BMS ion beams were collected using a mix of Faraday cups and ion counters. The laser was fired at a frequency of 5 Hz, with energies of 1–2 mJ/pulse and a spot size of 20–80 μm. During ablation runs, the PGE-A standard was also analyzed between samples to monitor drift in the Faraday cups and ion counters. These variations typically were less than 0.1% over a long day's analytical session. During the analyses, a dry aerosol of Ir was bled into the gas line between the ablation cell and the ICP-MS to provide a mass–bias correction with a precision independent of the abundance of Os in the unknown. In this routine, the overlap of ^{187}Re on ^{187}Os was also corrected by measuring the ^{185}Re peak and using $^{187}Re/^{185}Re = 1.6742$ and all the analyzed grains also had $^{187}Re/^{188}Os < 0.5$, ensuring that the isobaric interference of ^{187}Re on ^{187}Os was precisely corrected. The data were collected using the Nu Plasma time-resolved software, which allows selection of the most stable intervals of the signal for integration. The selected interval was divided into 40 replicates to provide a measure of the standard error. Under the ablation conditions described above, for sulfide grains having sizes of ≈50 μm and an average Os contents of ≈45 ppm, which is much lower than the Os content of the PGE-A standard (i.e., 200 ppm), a typical run duration of 100 s was achieved and a signal intensity of Os between 0.01 and 0.23 V, giving a precision for $^{187}Os/^{188}Os$ ranging from 3.60×10^{-4} to 2.60×10^{-3} (2SE).

The Os isotope compositions of the PGM and BMS s can be recast as model ages, i.e., T_{MA} and T_{RD} to reveal sequential events of mantle melting [67]. The T_{MA} model age represents the time of separation from a chondritic mantle reservoir calculated using the measured Re/Os ratio of the sulfide whereas T_{RD} (Re-depletion model age) assumes complete removal of Re (zero Re/Os) during melting, and is a minimum age for separation from a chondritic reservoir. Both types of model ages are dependent on the model reservoir selected to represent Os evolution in the upper mantle. In this study, we used the Enstatite Chondritic Reservoir (ECR) (present-day $^{187}Os/^{188}Os = 0.1281$ and $^{187}Re/^{188}Os = 0.421$; [68]), which has been demonstrated by independent geochronological data to be the best model for the Os-isotope evolution of the lithospheric mantle [32]. The quoted uncertainties on model ages include the uncertainties in the measured $^{187}Os/^{188}Os$ and $^{187}Re/^{188}Os$, calculated according to the equation of [69]. This estimate of the model age uncertainty does not take in account the uncertainty of the values for the chondritic reservoir, but this does not change the relative position of age peaks. In this study, the Os model ages were calculated relative to the Os-isotope evolution of Enstatite Chondrite (present day $^{187}Os/^{188}Os = 0.1281$, $^{187}Re/^{188}Os = 0.421$; [68]), which has been demonstrated to be the most accurate for studying the Os isotopic evolution of PGM in ophiolitic mantle [32,37,38]. In situ LA-MC-ICP-MS analyses for Re-Os isotopes of PGM and BMS are listed in Tables S4 and S5.

4. Results

4.1. Geochemistry of Chromite in Chromitite

Chromite from the studied samples lacks secondary alteration. Electron microprobe analyses of these chromite grains in the samples studied in this work yield Cr_2O_3 contents of 58.70–59.72 wt.% with a correspondingly high Cr# [Cr/(Cr + Al) atomic ratio; 0.76–0.77] and TiO_2 < 0.19 wt.%, which overlaps the compositional field for typical podiform (ophiolitic) chromitites (Figure 2a–d; Table S1).

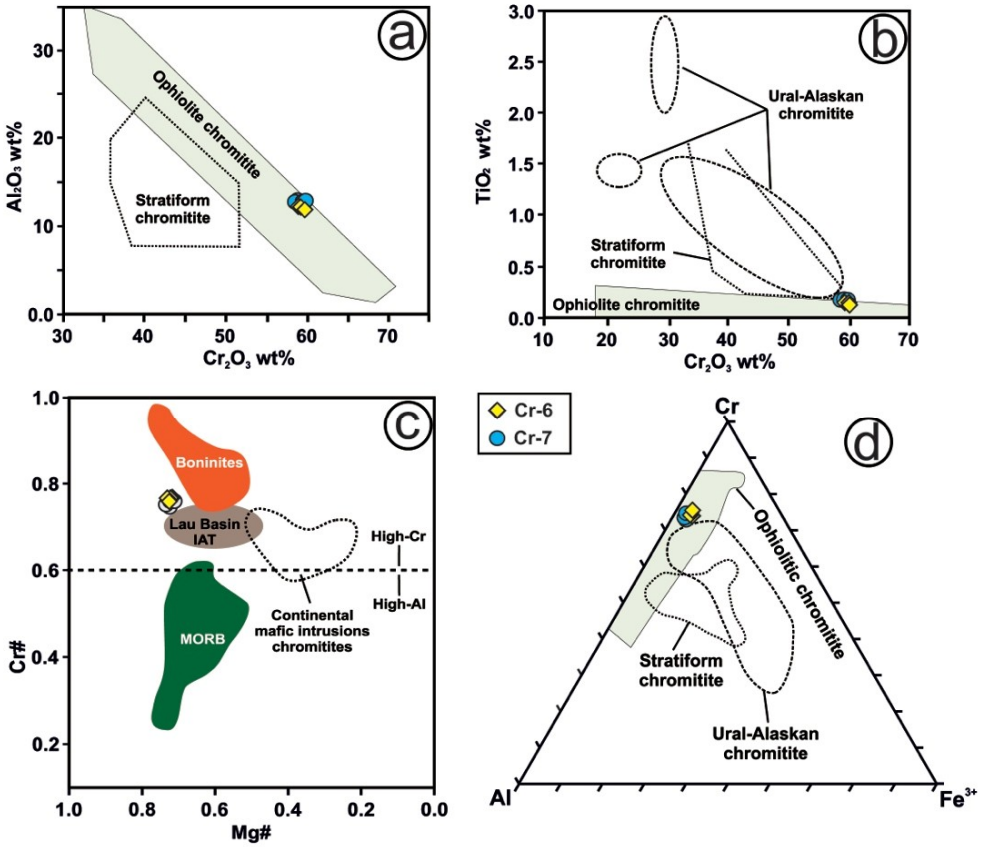

Figure 2. Chemical composition of chromite forming the North Andaman chromitites in terms of: (**a**) Al_2O_3 versus Cr_2O_3 (wt.%); (**b**) TiO_2 versus Cr_2O_3 (wt.%); (**c**) Cr# [(Cr/Cr + Al) atomic ratio] versus Mg# [(Mg/Mg + Fe^{2+}) atomic ratio]; (**d**) Fe^{3+}—Cr—Al (atomic element) ternary diagram. Data sources for chromian spinel of different tectonic settings are from [64,70]. Legend is inset in the figure.

Laser ablation ICP-MS analyses of chromite from these Andaman samples yielded contents of the minor- and trace-elements that are also similar to those of other high-Cr chromitites (Figure 3a–h). They are characterized by smaller amounts of Sc (<4.6–7.7 ppm), Ga (18–23 ppm), Co (158–212 ppm) and Zn (332–445 ppm) than V (463–637 ppm) and Mn (879–1018 ppm) (Table S2).

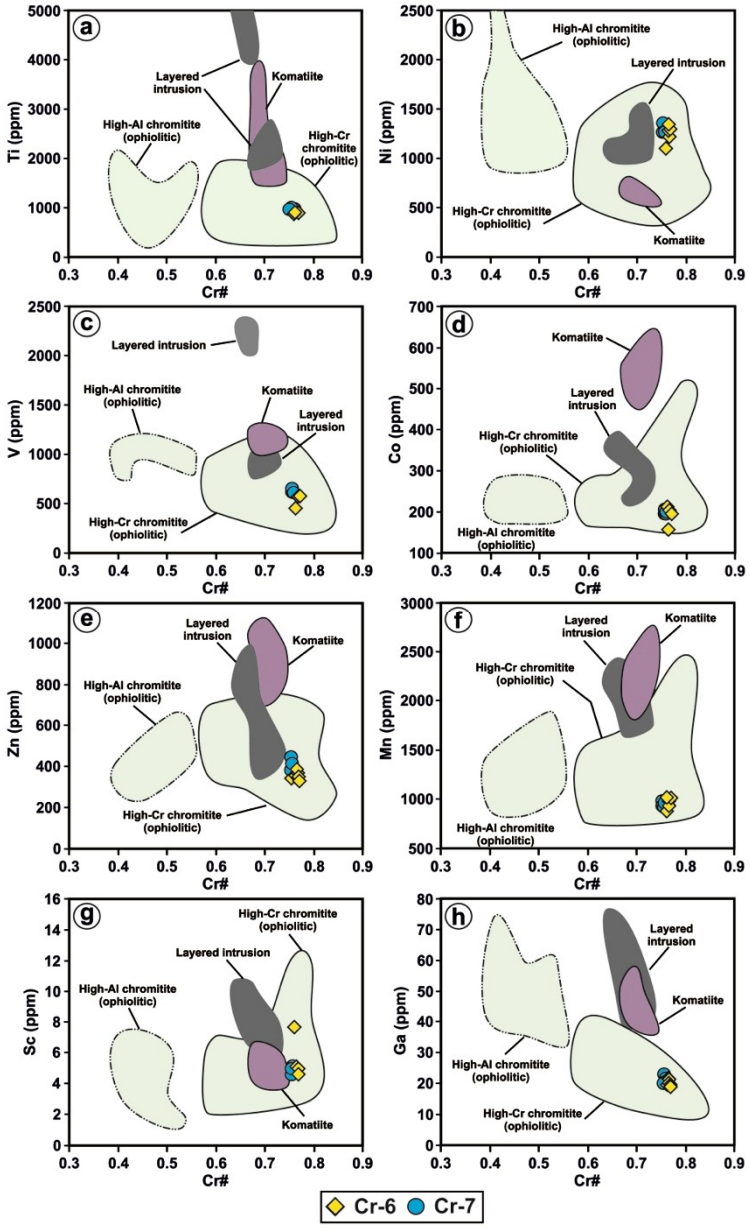

Figure 3. Compositional variation in terms of Cr# vs. (**a**) Ti, (**b**) Ni, (**c**) V, (**d**) Co, (**e**) Zn, (**f**) Mn, (**g**) Sc and (**h**) Ga in chromites from the Andaman ophiolite chromitites. Data sources for the compositional fields of other worldwide chromitites and accessory chromite from komatiites are from [12].

4.2. Elememtal and Isotopic Composition of Platinum-Group Minerals in Chromitite

The platinum-group minerals in the chromitite comprises tiny (<25 μm) grains of laurite (RuS_2) found as isolated single inclusions within chromite crystals or composite inclusions of laurite plus Os-Ir alloy and/or millerite (Figure 4a–d).

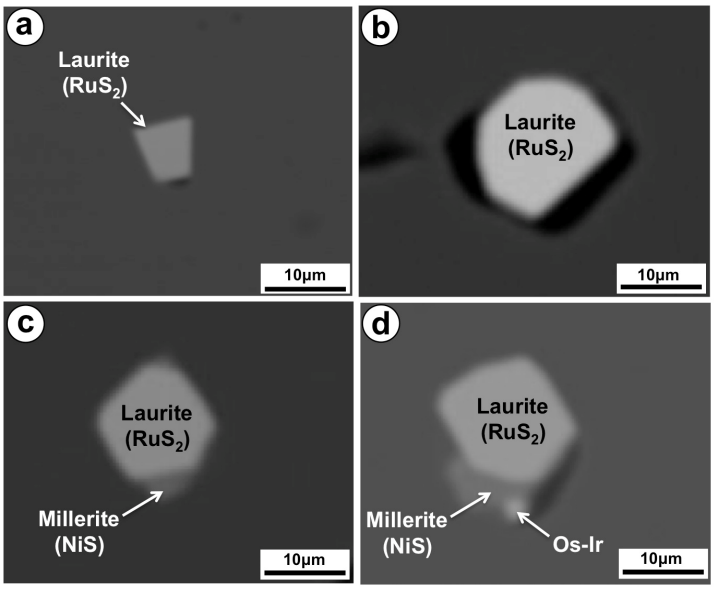

Figure 4. **(a–d)** Backscattered electron images of platinum-group mineral grains and associated millerite in unaltered chromite grains of the North Andaman chromitites.

Grains of laurite are Os-poor [$(Ru_{0.66}Os_{0.21}Ir_{0.08}Rh_{0.01}Fe_{0.03}Ni_{0.01})_{\sum=1.00}$ $S_{2.00}$] similar to other laurite hosted in other ophiolitic chromitites worldwide. There is no zoning and these grains exhibit a very homogenous intra-grain composition in terms of the Ru/Os ratio (Figure 5; Table S3).

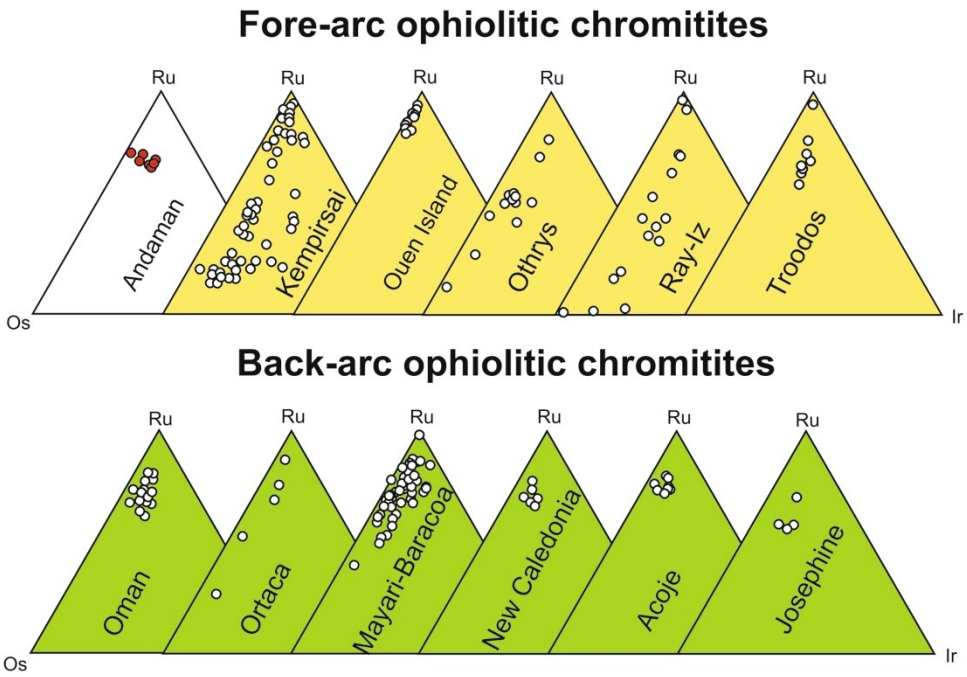

Figure 5. Composition of inclusions of laurite analyzed in this study and comparison with those minerals of the laurite (RuS_2)–erlichmanite (OsS_2) solid solution series in chromite grains in chromitites from different ophiolite complexes, plotted in Ru-Os-Ir (atomic %) ternary diagrams. The data for these plots are from the compilation by [71].

In situ LA-MC-ICP-MS analyses of 24 laurite grains reveal variability in the Os-isotopic compositions among grains in a single thin section. The $^{187}Re/^{188}Os$ ratio is very low in most grains (0.0004 ± 0.0001; 2σ uncertainty; Figure 6a and Table S4), thus yielding $T_{MA} \approx T_{RD}$ model

ages that span between 320 and 1000 Ma and cluster around single peaks at 0.5 Ga and 1.0 Ga (see cumulative plot in Figure 6b). The $^{187}Os/^{188}Os$ ratios vary from 0.1259 ± 0.0003 to 0.1210 ± 0.0008 (2σ uncertainty; Figure 6a).

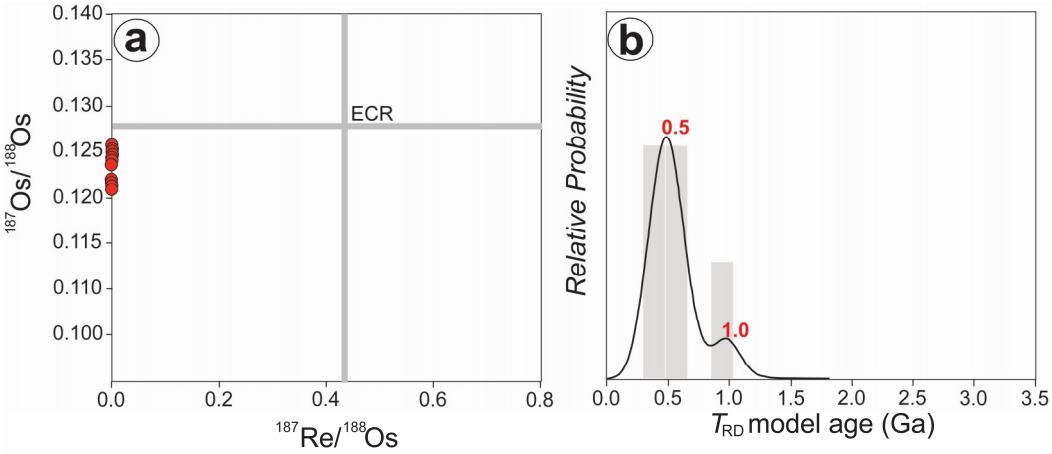

Figure 6. Re-Os isotope systematics in the analyzed laurites (n = 24 grains) of the North Andaman chromitites in terms of: (**a**) Isotopic ratios $^{187}Re/^{188}Os$ and $^{187}Os/^{188}Os$; (**b**) Cumulative-probability plots and histograms (shaded bars, relative probability) of Os model ages (Ga) where uncertainties artificially were increased to 0.1 Ga to allow for uncertainty in the enstatite chondritic reservoir (ECR) model-age reference curve. This plot is most appropriate for estimates of the *absolute* depletion ages of different mantle domains, and for comparison between datasets from platinum-group minerals (PGM) and base-metal sulfides (BMS).

4.3. Isotopic Compositions of Base-Metal Sulfides in Peridotites

Base-metal sulfides in the peridotites are all pentlandite, which were identified under reflected light and qualitatively by means of their characteristic Energy-dispersive X-ray (EDS) spectra acquired by a Scanning Electron Microscope (SEM). These grains are much larger than the PGM identified in the chromitite, with sizes varying from 50 to 500 µm, and exhibit typical droplet (Figure 7a) or holly-leaf morphology interstitial to the silicate minerals (Figure 7b).

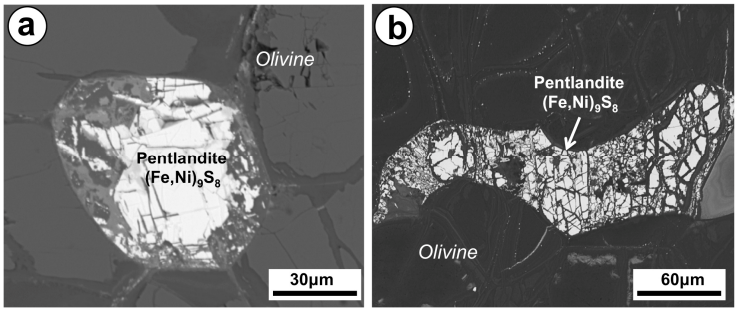

Figure 7. (**a**,**b**) Backscattered electron images of pentlandite grains in peridotites hosting the North Andaman chromitites.

All the BMS (37) grains analyzed in situ by LA-MC-ICP-MS have subchondritic $^{187}Re/^{188}Os$ (<0.421; ECR; [68]) and $^{187}Os/^{188}Os$ between 0.10800 ± 0.00011 and 0.12535 ± 0.00010 (Figure 8a; Table S5). In general, there is no correlation between the $^{187}Re/^{188}Os$ and $^{187}Os/^{188}Os$, although significant variation in these isotopic ratios and Os model ages (main peaks at ~0.5, 1.2, 1.8, 2.1 and 2.5 Ga) can be observed between grains separated a few millimeters within a single thin section (Figure 8b; Table S5).

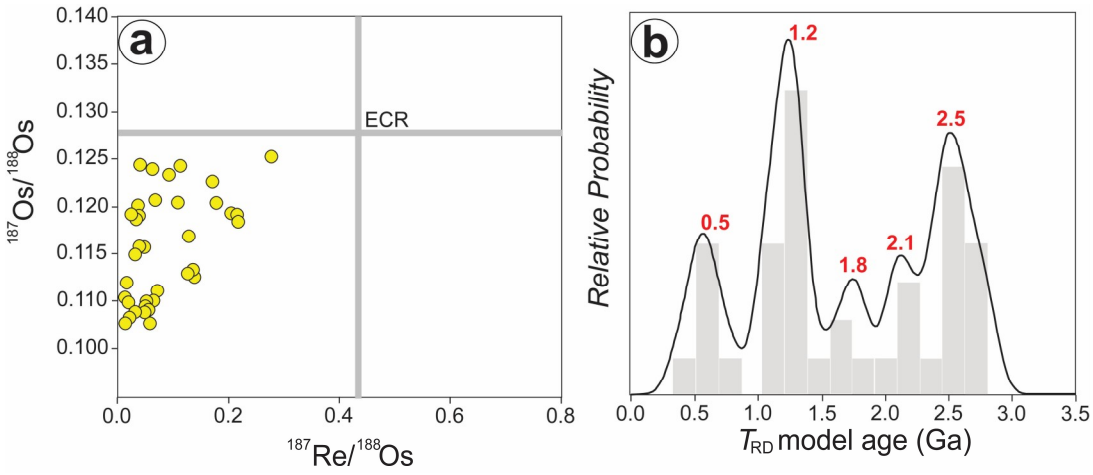

Figure 8. Re-Os isotope systematics in the analyzed pentlandite (n = 37 grains) of the North Andaman lherolites hosting the chromitites in terms of: (**a**) Isotopic ratios $^{187}Re/^{188}Os$ and $^{187}Os/^{188}Os$; (**b**) Cumulative-probability plots and histograms (shaded bars, relative probability) of Os model ages (Ga) where uncertainties artificially were increased to 0.1 Ga to allow for uncertainty in the ECR model-age reference curve. This plot is most appropriate for estimates of the *absolute* depletion ages of different mantle domains, and for comparison between datasets from BMS and PGM.

5. Discussion

5.1. Genesis of the Andaman Chromitites in the Upper Mantle

Pioneering models suggested the formation of chromitite and host dunite at low pressures in the uppermost part of the mantle in oceanic settings as a result of the disequilibrium reaction of mantle peridotites with foreign melts [4,5]. Crystallization of chromite in such scenarios is interpreted to be the result of the small-scale mingling of basaltic melts that had different SiO_2 contents within dunite representing melt–flow channels [6–9]. The identification of minerals that typically form in the continental crust (e.g., zircon, quartz, K-feldspar, almandine, andalusite, apatite and kyanite) in some mantle-hosted chromitites links the aforementioned foreign melts to subduction processes, where crustal material is delivered into the mantle at subduction zones and is then returned to the crust as a component of mantle-derived magmas [10–13]. The mechanisms of transfer of these crustal minerals from the subducting slab to the overlying mantle wedge beneath intra-oceanic volcanic arcs where the parental melts of the chromitite are formed include: (1) slab window created in subducted slab during subduction initiation, allowing underlying asthenosphere and melts to rise in order to generate Cr-rich mafic magmas [14,15] or (2) cold plumes comprising partially molten hydrated peridotite, dry solid mantle, and subducted oceanic crust able to generate the melts necessary for chromitite formation [12,13]. In some chromitites (e.g., Tibet, Northwestern Mexico), however, these recycled crustal minerals coexist with minerals that typically form under super-reducing conditions (e.g., native elements, alloys, carbides, nitrides; known as SuR assemblage [16]) and/or at ultra-high pressures (UHP $\geq$ 0.4 GPa; diamond, TiO_2 II, stishovite pseudomorphs). Some authors [12,16–20] suggested that such mixtures of crustal minerals and the mantle SuR and UHP assemblages reflect a complex evolutionary history of the chromitites in the upper mantle. An initial stage of formation of chromitite might involve a melt–rock reaction and subsequent melt–melt mixing processes in mantle wedges above a subducting slabs, followed by subduction to the Mantle Transition Zone where they become metamorphosed at UHP conditions, and finally return back to the surface with their host dunite/harzburgite at spreading centers as mantle diapirs. The proposed recycling of chromitites is apparently recorded in the chromite by exsolution of pyroxenes and coesite, suggesting inversion from a high-P polymorph of chromite [17,21] and by the evidence for inclusions of the high-pressure polymorph of olivine (wadsleyite) in chromites from the Luobusa ultramafic body in Tibet [22]. Alternative models [23–27] involve mantle plumes

which originate from the lower mantle through the MTZ or directly from the MTZ, rise while collecting a mixture of crustal materials and super-reducing minerals from the transition zone. These are then carried though the upper mantle by an upwelling plume to be incorporated in the magma that is generated beneath a spreading system. The interaction of deep-seated plumes with subduction zone peridotite has also been suggested to explain the origin of some chromitites hosted in the mantle section of ophiolites from the Dominican Republic [28]. Recent works by [29] and [30] based on the study of chromitites from the eastern Cuban and Central Mexican ophiolites showed that some minerals of the super-reducing and ultrahigh-pressure (SuR-UHP) assemblages do not necessarily form at the mantle transition zone but they may easily form during serpentinization-related processes. Therefore, a low-pressure origin of chromitites in the suprasubduction mantle beneath intra-oceanic island arcs seems to be a common scenario for ophiolitic chromitites, although there is still much debate about the complex processes involved in the generation of mantle-hosted chromitites [3,28].

Chromite forming the Andaman chromitite has relatively high Cr_2O_3, and low Fe_2O_3 and TiO_2 contents, overlapping the range typical for chromitite from chromitites hosted in the mantle sequence of ophiolite complexes (Figure 2a–d). This chemical composition also correlates well with the chemistry of chromian spinel from arc sources (Figure 9a–c). In addition, we did not identify minerals diagnostic of the SuR or UHP assemblages in the Andaman chromitites, suggesting that they are ordinary (low-pressure) chromitites such as those defined by [17].

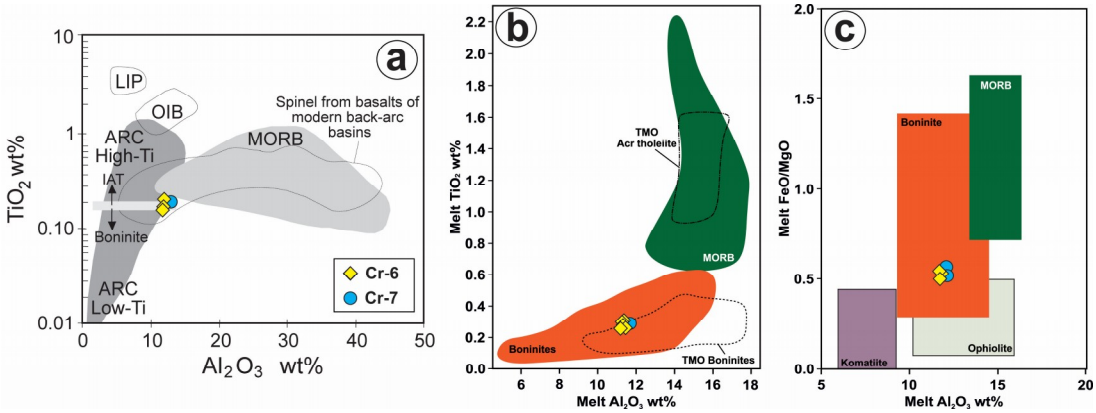

Figure 9. (**a**) Chemical composition of chromite forming the North Andaman chromitites in terms of TiO_2 versus Al_2O_3 (wt.%); (**b**,**c**) composition of the parental melt in equilibrium with the studied chromitite in terms of TiO_2 versus Al_2O_3 (wt.%) and ratio FeO/MgO versus Al_2O_3 (wt.%) respectively. Data sources for chromian spinel of different tectonic settings are from [64,70,72]. Legend is inset in the figure. Keys for figure (a): LIP (Large Igneous Provinces), OIB (Ocean Island Basalts), MORB (Mid-ocean Ridge Basalts).

The calculation of the parental melt compositions indicates that the melts that produced the chromite of the Andaman chromitites contained 11–12 wt.% Al_2O_3 and relatively low TiO_2 (between 0.25 and 0.30 wt.%), with FeO/MgO ratios varying between 0.51 and 0.57. This composition is akin to high-Mg island arc tholeiite (IAT) and boninites and broadly similar to that previously estimated by [48] for chromitites from Rutland Island, located nearly 300 km south of the present study area, as well as other suprasubduction-zone podiform chromitites (Table S6). Chromites crystallized from melts with identical Al_2O_3 contents to those analyzed here are known to constitute the high-Cr chromitites from the suprasubduction zone ophiolite of Kempirsai–Batamshink in Kazakhstan [6], the Mayarí Massif in Cuba [12], and the podiform chromitites of the fore-arc ophiolite of Thetford Mines in Canada [72]. All these chromitites were interpreted to have formed in the shallow upper mantle, within the mantle–crust transition zone (i.e., Moho Transition Zone).

The idea that the podiform chromitites at Andaman were formed from high-Mg IAT and/or boninitic melt within a fore-arc setting is also supported by the distribution of minor elements in

chromite. Figure 10 shows the composition of the studied chromitites and other known chromitites formed in both fore-arc and back-arc setting in intra-oceanic arcs. Remarkably, the MORB-normalized minor- and trace-element patterns of the Andaman chromites are very similar to those of the high-Cr chromites in low-pressure chromitites from fore-arc oceanic supra-subduction zone (SSZ) mantle but distinctively different (higher Sc and lower Ga) from high-Cr and high-Al chromites formed in back-arc settings.

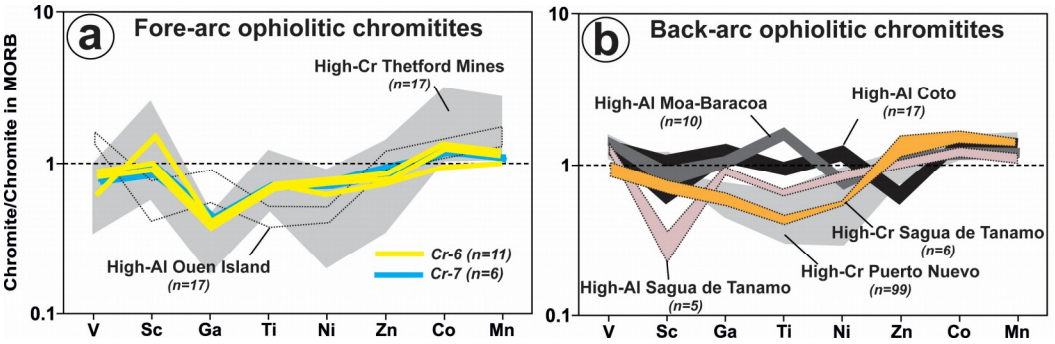

Figure 10. Spider diagrams showing the composition of minor- and trace-elements of chromites from chromitites of the two chromitite bodies analyzed in this study from the North Andaman ophiolite. Comparisons with other low-pressure chromitites from supra-subduction zone ophiolites in fore-arc and back-arc regions are shown in (**a**,**b**) respectively. Data sources for high-Cr chromitites of the Thetford Mine ophiolite are from [72] and those for the high-Al chromitites of Ouen Island in New Caledonia are from [73]. Data for high-Al and high-Cr chromitites from back-arc regions in ophiolites are taken from the compilation by [12].

It is important to note that the chromitites studied here are hosted within dunite melt channels diking lherzolites [43,44] rather than depleted or ultra-depleted harzburgite as observed in most ophiolites worldwide [2,3]. This association of the chromitite–dunite pair with lherzolites in the ophiolitic mantle is relatively uncommon in ophiolites, and it has been reported only in the massif of Poum, in the New Caledonia ophiolite, where high-Cr and high-Al chromitite were found associated with a paleo-transform fault [74], Kallidromon ophiolite in Greece [75,76] Troodos ophiolite in Cyprus [77]. Other examples include chromitites hosted in dunite diking orogenic lherzolites of the Ronda and Ojén massifs in southern Spain [41]. In the latter case, the chromitites formed in lherzolites of a subcontinental lithospheric mantle were exhumed by the opening of a back-arc basin above the suprasubduction zone. In both the oceanic and subcontinental mantle, the chromitite–dunite pair was explained as a product of the metasomatic reaction of infiltrating deeper mantle melt and peridotite and subsequent melt mixing within these replacive dunite, which represent conduits for melt transport [2,3,12,41]. In this model, Cr is supplied to the infiltrating melt by the decomposition of pyroxenes, a phenomenon effective at relatively low pressures [78]. In the Andaman mantle, pyroxenes could exhaust when pulses of SiO_2-undersaturated high-Mg IAT melts migrated through the mantle peridotite, thus generating dunite sheaths and a secondary melt with a local boninitic affinity, very likely following the reaction proposed by [3]: SiO_2-poor melt + pyroxenes + hydrous phases → olivine + SiO_2-richer melt. A continuous supply of batches of primitive SiO_2-undersaturated melt may produce a self-sustaining system in which mixing of melts with variable degrees of fractionation enabled the precipitation of chromite within the dunite channels [2].

5.2. Significance of Re-Os Data in Platinum Group Minerals and Base-Metal Sulfides

The laurite grains documented in this study are hosted in unaltered chromite grains and exhibit subchondritic $^{187}Os/^{188}Os$ and $^{187}Re/^{188}Os$ (Figure 6a; Table S4). These textural and isotopic features suggest these PGM were encapsulated in chromite (an oxide with negligible Os contents) while leaving their Re-Os systematics undisturbed, so they did not interact with external Re-Os-bearing

fluids [18,38,79,80]. Likewise, the absence of highly radiogenic isotopic ratios shows that the PGM were not significantly affected by interaction with melts derived from outer core-related reservoirs (i.e., deep-rooted plumes; [81]). Therefore, the measured $^{187}Os/^{188}Os$ ratios in these PGM are reliable records of the Os isotope signatures of their original sources within the framework of the convecting mantle.

Overall, the analyzed laurite grains exhibit a variability of $^{187}Os/^{188}Os$ that overlaps the range of laurites hosted in grains of magmatic chromite from ophiolitic chromitites elsewhere (Figure 11).

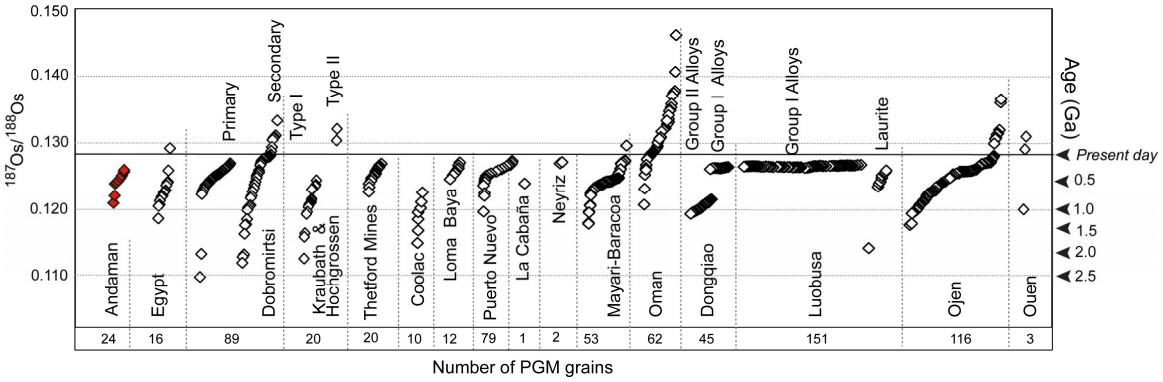

Figure 11. $^{187}Os/^{188}Os$ isotopic ratios and corresponding T_{RD} model ages for PGM analyzed in this study (red diamonds) and other analyzed in situ in chromitites from ophiolite worldwide; updated after [71].

Differences in the $^{187}Os/^{188}Os$ composition of laurite grains within a single chromitite body can, in principle, be accounted for by different initial Re/Os in the melt from which laurite is eventually crystallized. Experimental studies indicate that at P-fO_2-fS_2-T conditions relevant for the crystallization of chromitites in the upper mantle, laurite with compositions similar to those reported in this study can crystallize in equilibrium with Os-Ir alloy at 1200–1300 °C and log fS_2 from −2 to −1.3 [82–84]. In this scenario, laurite crystallizing from a melt with relatively high initial Re/Os ratio may over time be enriched in the radiogenic daughter ^{187}Os, whereas those grains acquiring lower initial Re/Os ratios should produce less radiogenic $^{187}Os/^{188}Os$. However, experimental results have shown that magmatic laurite exhibits limited Re uptake [84], therefore displaying a tendency to have very low initial Re/Os which allows little ^{187}Os ingrowth upon ^{187}Re decay. This crystal-partitioning effect is remarkable if laurite coexists with other PGM (e.g., Os-Ir alloys) or BMS, which preferentially partition Re from the melt resulting in higher $^{187}Os/^{188}Os$ than coexisting laurite [79,84,85]. Interestingly, some laurite grains identified in this study coexist with Os-Ir alloys and/or millerite (Figure 4c,d), suggesting the input of relatively more radiogenic $^{187}Os/^{188}Os$ ratios from these minerals in the signals collected during single-spot LA-MC-ICPMS analysis.

Alternatively, the observed dispersion of $^{187}Os/^{188}Os$ among the analyzed individual laurite grains could reflect their crystallization from different batches of basaltic melts with distinct Os-isotopic compositions, which had already been derived from a heterogeneous mantle source [37,86]. In this scenario, the laurite grains and their coexisting Os-Ir alloys and millerite should acquire different Re/Os ratios representative of the melts from which they crystallized, rather than only the effects of crystal fractionation of Re and Os among these minerals. According to experimental data on the metal–sulphide equilibrium in the Ni-Fe-S system [87], a high-temperature polymorph of millerite α-NiS could form between 1000 and 1200 °C but at relatively higher sulfur fugacity (log fS_2 from −0.5 to 1) than estimated for the crystallization of laurite and Os-Ir alloys. A mechanism involving mixing (or mingling) of individual basaltic melts with contrasting physicochemical properties (i.e., different Si contents) might create a heterogeneous environment with variable temperature and fS_2 that promotes the local segregation of immiscible sulfide liquids contemporaneously with laurite and Os-Ir alloys [2].

As noted above, melt mixing or mingling within dunite conduits is also the most probable mechanism for the genesis of the Andaman chromitites.

These two models proposed above assume ab initio that PGM and millerite crystallized directly from the basaltic melt(s) from which chromitite crystallized. However, experimental [88] and empirical work [89] has shown that laurite and Ru-Os-Ir alloys may also form as a result of partial melting (>1000 °C) of BMS subjected to decreasing fS_2. According to these researchers, Os-rich alloys should be released during the highest percentages of melting necessary for the exhaustion of BMS, which usually occurs in mantle peridotites at >20–30% depending on temperature, pressure and sulfur abundance at the onset of melting. In contrast, lower rates of partial melting over the last five percent of melting prior to complete consumption of the BMS are expected to facilitate the exsolution of laurite from the mantle BMS instead the IPGE alloys [89].

These experimental and empirical results support the idea that some laurite (and Os-Ir alloy) now hosted in chromite from the Andaman chromitites could also form at the expense of a high-temperature base-metal sulfide subjected to decreasing fS_2 during partial melting of pyroxenes from the host lherzolite that originated the dunite channels. Therefore, not all the PGM now hosted in the Andaman chromitites were necessarily formed by direct precipitation from the basaltic melt parental to the chromitite. Some of them could represent grains that were physically entrained by a melt that was extracted from the sulfides in the source peridotite or during melt–rock reactions associated to the migration of this melt through the mantle peridotite. Interestingly, all the laurite grains analyzed here yield Os model ages much older than crystallization age of the igneous rocks in the Andaman ophiolite (95 Ma), suggesting that they provide the insights of melt depletion or metasomatic events predating the chromitite formation. Ancient laurite grains have been found associated with younger metasomatic sulfides in fertile lherzolites from the Lherz massif [90]. Indeed, laurites now found hosted in the chromitites might represent exotic material, not belonging to the local oceanic mantle lithosphere [32,40] but the subcontinental lithosphere or sub-arc mantle wedge.

It is worth noting that laurite exhibiting Re-Os isotope model age-peaks older than the supposed age of chromitite formation in the mantle section of ophiolites has already been reported worldwide (see review by [71]) and previously interpreted as reflecting that these PGM inherited the Os-isotopic signature of older events that affected the host mantle peridotite (e.g., [37]). In fact, laurites from chromitite and pentlandite from host peridotite analyzed in this study preserve two common Os model age peaks at ≈0.5 and 0.1 Ga (Figure 6a,b and Figure 8a,b). The latter BMS also show a wide variation in Re/Os ratios as is typical of the BMS found in upper mantle peridotites that have experienced a multistage history of melt depletion or metasomatism. In mantle peridotites, only those sulfides with $^{187}Re/^{188}Os < 0.07–0.08$ can be regarded as isotopically "undisturbed" and representative of real melting/refertilization events in the mantle [91,92]. Most (24/37) of our pentlandite grains have $^{187}Re/^{188}Os < 0.08$ (Figure 8a; Table S5), whereas the remaining grains still yield subchondritic $^{187}Re/^{188}Os = 0.1–0.28$. The latter grains yield $T_{MA} \approx T_{RD}$ as is typical of grains with relatively undisturbed Re-Os signature, which still preserve their original $^{187}Os/^{188}Os$ ratios. Therefore, for all those sulfides, the zero-Re assumption used in the calculation of T_{RD} is probably valid, and they provide meaningful Os model ages with useful chronological information on tectonothermal events in the mantle.

5.3. Interpretation of Os Model Ages

As noted in the previous section the Os isotopes measured in laurite from chromitite and pentlandite from peridotite can be used to constrain the nature and age of depletion and metasomatism events of the Andaman upper mantle. Figures 6b and 8b display the distribution of T_{RD} model ages in individual grains of laurite from chromitites and pentlandite from host peridotites from Andaman, which exhibits a multistage evolution of the upper mantle that extends back to 2.5 Ga. The T_{RD} ages calculated for laurites cluster around two main peaks: ≈0.5 and 1.0 Ga whereas the distribution of T_{RD} in pentlandites show five major peaks at ≈0.5, 1.2, 1.8, 2.1 and 2.5 Ga. Considering the

uncertainties inherent in model ages calculations, they collectively match well with zircon U-Pb ages of tectonothermal events at ≈0.5, 1.0, 1.8 and 2.5 Ga within the Indian Plate [93]. Although the total number of analyses of laurite is too small to be statistically robust, there is an interesting correlation with the data obtained for pentlandite from the host peridotite. The most recent peaks in both the distributions correspond to the Cambrian (≈0.5 Ga) and to the Mesoproterozoic–Neoproterozoic boundary (≈1.0 Ga). The younger age ~0.5 Ga may be correlated with the Pan-African orogeny that deformed the ancient Dharwar and Singhbhum cratons and the Eastern Ghats mobile belt forming the South Indian block. Likewise, the age peaks at 2.5, 2.1 and 1.8 Ga identified in the PGM-BMS analyzed here match with the magmatic events that resulted in the intrusion of different generations of dike swarms of mafic rocks and tonalite–trondhjemite–granodiorite (TTG) gneiss between ≈2.5 and ≈2.0–1.8 Ga ago into the Neoarchean greenstone belts (2.7 Ga) of the Dharwar craton [93–97]. Grenvillian ages of ≈1.2 Ga identified in our Os-model age dataset also fit with the Cuddapah orogeny and also recorded in the granulites of the Eastern Ghats Belt [98].

All these ages are clearly older than the supposed Cretaceous age of the igneous rocks in the ophiolite sequence of the Andaman Islands. It is worth noting that old tectonothermal events have previously been recognized in chromitites and host peridotites from modern oceanic lithosphere and Phanerozoic ophiolites [11,18,32,37,40]. These ages have been interpreted to reflect large-scale isotopic heterogeneities (i.e., the coexistence of variably Re-depleted reservoirs; [99–101]) and/or the presence of ancient subcontinental lithospheric domains (or at least ribbons of them) within the oceanic upper mantle [91]. Geophysical evidence and geochemical tomography of the oceanic mantle seems to support the second alternative, as rigid (buoyant) fragments of cratonic subcontinental lithospheric mantle (SCLM) have been found embedded in the oceanic lithosphere [101]. Therefore, we suggest that in the context of convergence of the Indian and Eurasian plate during the Mesozoic to Tertiary, dismembered blocks of ancient SCLM could have spread, colliding with passive margins (e.g., Sino-Burma microcontinent; [102] and references therein), and thus contributing to the development of the subduction-related Andaman–Java volcanic arc. We suggest that these major tectonic events have stripped off most of the old continental crust, leaving behind the residues of an ancient subcontinental mantle now signaled by the osmium isotopes of the Andaman chromitites and host lherzolites.

Supplementary Materials: The following are available online at http://www.mdpi.com/2075-163X/10/8/686/s1, Table S1: EPMA analyses of chromite from Andaman chromitites, Table S2: EPMA analyses of the studied laurite from Andaman chromitites, Table S3: In situ LA-ICP-MS data of minor and trace elements of chromite from Andaman chromitites, Table S4: In situ LA-ICP-MS Re-Os data of laurite from Andaman chromitites, Table S5: In situ LA-ICP-MS Re-Os data of pentlandite from Andaman chromitite, Table S6: Calculation of Al_2O_3 and TiO_2 contents and FeO/MgO ratios of the melts in equilibrium with chromite from the samples analyzed in this study and other mantled hosted "podiform" array high-Cr chromitites of the literature.

Author Contributions: This work include contributions from all the authors who have worked as a team collecting samples, acquiring data and sourcing ideas that inspired the interpretations and models provided in this manuscript. Finally, all the authors revised the writing style of the manuscript. Specifically, J.M.G.-J. and S.K.M. conceived and designed the study while B.G. provided the samples. The EMPA and SEM analytical work was carried out largely by J.M.G.-J. whereas the in situ analysis of sulfides at University of Chicoutimi was carried out by J.M.G.-J. under the supervision of W.L.G. All the authors analyzed and discussed the data, and revised the manuscript, which was written by J.M.G.-J. and S.Y.O. All authors have read and agreed to the published version of the manuscript.

Funding: This research was supported by Australian Research Council (ARC) grants to SO'R, WLG and NJP prior to 2011 and subsequently by the ARC Centre of Excellence for Core to Crust Fluid Systems (CCFS). Additional funding for instrumental analysis was provided by the Spanish projects RTI2018-099157-A-I00, granted by the "Ministerio de Ciencia, Innovación y Universidades" and Ministerio de Economía y Competitividad" (MINECO) and the Ramón y Cajal Fellowship RYC-2015-17596 to JMGJ. An important volume of the analytical data were obtained using instrumentation funded by DEST Systemic Infrastructure Grants, ARC LIEF, NCRIS/AuScope, industry partners and Macquarie University. This is contribution 1521 from the ARC Centre of Excellence for Core to Crust Fluid Systems (http://www.ccfs.mq.edu.au) and 1398 in the GEMOC Key Centre (http://www.gemoc.mq.edu.au) and it is also related to IGCP-662.

Acknowledgments: The authors are indebted to Norman J. Pearson for his careful help with LA-ICP-MS. We also acknowledge Kreshimir N. Malitch and two anonymous referees for their constructive criticism, which greatly helped to improve this manuscript.

Conflicts of Interest: The authors declare no conflict of interest.

References

1. Leblanc, M.; Nicolas, A. Ophiolitic chromitites. *Int. Geol. Rev.* **1992**, *34*, 653–686. [CrossRef]
2. González-Jiménez, J.M.; Griffin, W.L.; Proenza, J.A.; Gervilla, F.; O'Reilly, S.Y.; Akbulut, M.; Pearson, N.J.; Arai, S. Chromitites in ophiolites: How, where, when, why? Part II. The crystallisation of chromitites. *Lithos* **2014**, *189*, 140–158. [CrossRef]
3. Arai, S.; Miura, M. Formation and modification of chromitites in the mantle. *Lithos* **2016**, *264*, 277–295. [CrossRef]
4. Arai, S.; Abe, N. Reaction of orthopyroxene in peridotite xenoliths with alkali basalt melt and its implications for genesis of alpine-type chromitite. *Am. Mineral.* **1995**, *80*, 1041–1047. [CrossRef]
5. Zhou, M.F.; Robinson, P.T.; Bai, W.J. Formation of podiform chromites by melt–rock interaction in the upper mantle. *Mineral. Depos.* **1994**, *29*, 98–101. [CrossRef]
6. Melcher, F.; Grum, W.; Simon, G.; Thalhammer, T.V.; Stumpfl, E.F. Petrogenesis of the ophiolitic giant chromite deposits of Kempirsai, Kazakhstan: A study of solid and fluid inclusions in chromite. *J. Petrol.* **1997**, *38*, 1419–1458. [CrossRef]
7. Proenza, J.A.; Gervilla, F.; Melgarejo, J.C.; Bodinier, J.L. Al- and Cr-rich chromitites from the Mayarí–Baracoa Ophiolitic Belt (Eastern Cuba): Consequence of interaction between volatile-rich melts and peridotites in suprasubduction mantle. *Econ. Geol.* **1999**, *94*, 547–566. [CrossRef]
8. Gervilla, F.; Proenza, J.A.; Frei, R.; González-Jiménez, J.M.; Garrido, C.J.; Melgarejo, J.C.; Meibom, A.; Díaz-Martínez, R.; Lavaut, W. Distribution of platinum-group elements and Os isotopes in chromite ores from Mayarí–Baracoa Ophiolilte Belt (eastern Cuba). *Contrib. Mineral. Petrol.* **2005**, *150*, 589–607. [CrossRef]
9. González-Jiménez, J.M.; Griffin, W.L.; Gervilla, F.; Proenza, J.A.; O'Reilly, S.Y.; Pearson, N.J. Chromitites in ophiolites: How, where, when, why? Part I. Origin and significance of platinum-group minerals. *Lithos* **2014**, *189*, 127–139.
10. Yamamoto, S.; Komiya, T.; Yamamoto, H.; Kaneko, Y.; Terabayashi, M.; Katayama, I.; Iizuka, T.; Maruyama, S.; Yang, J.; Kon, Y.; et al. Recycled crustal zircons from podiform chromitites in the Luobusa ophiolite, southern Tibet. *Island Arc* **2013**, *22*, 89–103. [CrossRef]
11. Belousova, E.A.; González-Jiménez, J.M.; Graham, I.; Griffin, W.L.; O'Reilly, S.Y.; Pearson, N.; Martin, L.; Craven, S. The enigma of crustal zircons in upper mantle rocks: Clues from the Coolac ultramafic complex, SE Australia. *Geology* **2015**, *43*, 123–126. [CrossRef]
12. González-Jiménez, J.M.; Camprubí, A.; Colás, V.; Griffin, W.L.; Proenza, J.A.; O'Reilly, S.Y.; Centeno-García, E.; García-Casco, A.; Belousova, E.; Talavera, C.; et al. The recycling of chromitites in ophiolites from southwestern North America. *Lithos* **2017**, *294*, 53–72. [CrossRef]
13. Proenza, J.A.; González-Jiménez, J.M.; García-Casco, A.; Belousova, E.; Griffin, W.L.; Talavera, C.; Rojas-Agramonte, Y.; Aiglsperger, T.; Navarro-Ciurana, D.; Pujol-Solà, N.; et al. Cold plumes trigger contamination of oceanic mantle wedges with continental crust-derived sediments: Evidence from chromitite zircon grains of eastern Cuban Ophiolites. *Geosci. Front.* **2018**, in press. [CrossRef]
14. Zhou, M.F.; Robinson, P.T.; Su, B.X.; Gao, J.F.; Li, J.W.; Yang, J.S.; Malpas, J. Compositions of chromite, associated minerals, and parental magmas of podiform chromite deposits: The role of slab contamination of asthenospheric melts in suprasubduction zone environments. *Gondwana Res.* **2014**, *26*, 262–283. [CrossRef]
15. Robinson, P.T.; Trumbull, R.B.; Schmitt, A.; Yang, J.S.; Li, J.W.; Zhou, M.F.; Erzinger, J.; Dare, S.; Xiong, F. The origin and significance of crustal minerals in ophiolitic chromitites and peridotites. *Gondwana Res.* **2015**, *27*, 486–506. [CrossRef]
16. Griffin, W.L.; Afonso, J.C.; Belousova, E.A.; Gain, S.E.; Gong, X.H.; González-Jiménez, J.M.; Howell, D.; Huang, J.X.; McGowan, N.; Pearson, N.J.; et al. Mantle recycling: Transition zone metamorphism of Tibetan ophiolitic peridotites and its tectonic implications. *J. Petrol.* **2016**, *57*, 655–684. [CrossRef]
17. Arai, S. Possible recycled origin for ultrahigh-pressure chromitites in ophiolites. *J. Mineral. Petrol. Sci.* **2010**, *105*, 280–285. [CrossRef]
18. McGowan, N.M.; Griffin, W.L.; González-Jiménez, J.M.; Belousova, E.A.; Afonso, J.; Shi, R.; McCammon, C.A.; Pearson, N.J.; O'Reilly, S.Y. Tibetan chromitites: Excavating the slab graveyard. *Geology* **2015**, *43*, 179–182. [CrossRef]

19. Yamamoto, S.; Komiya, T.; Hirose, K.; Maruyama, S. Coesite and clinpyorexene exsolution lamellae in chromite: In-situ ultrahigh-pressure evidence from podiform chromitites in the Luobusa ophiolite, southern Tibet. *Earth Planet. Sci. Lett.* **2009**, *109*, 314–322.
20. Xiong, Q.; Griffin, W.L.; Huang, J.X.; Gain, S.E.; Toledo, V.; Pearson, N.J.; O'Reilly, S.Y. Super-reduced mineral assemblages in "ophiolitic" chromitites and peridotites: The view from Mount Carmel. *Eur. J. Mineral.* **2017**, *29*, 557–570. [CrossRef]
21. Zhang, Y.; Jin, Z.; Griffin, W.L.; Wang, C.; Wu, Y. High-pressure experiments provide insights into the Mantle Transition Zone history of chromitite in Tibetan ophiolites. *Earth Planet. Sci. Lett.* **2017**, *463*, 151–158. [CrossRef]
22. Satsukawa, T.; Griffin, W.L.; Piazolo, S.; O'Reilly, S.Y. Messengers from the deep: Fossil wadsleyite–chromite microstructures from the Mantle Transition Zone. *Sci. Rep.* **2015**, *5*, 16484. [CrossRef] [PubMed]
23. Ruskov, T.; Spirov, I.; Georgieva, M.; Yamamoto, S.; Green, H.W.; McCammon, C.A.; Dobrzhinetskaya, L.F. Mossbauer spectroscopy studies of the valence state of iron in chromite from the Luobusa massif of Tibet: Implications for a highly reduced deep mantle. *J. Metamorph. Geol.* **2010**, *28*, 551–560. [CrossRef]
24. Wu, Y.; Xu, M.; Jin, Z.; Fei, Y.; Robinson, P.T. Experimental constraints on the formation of the Tibetan podiform chromitites. *Lithos* **2016**, *245*, 109–117. [CrossRef]
25. Xiong, F.; Yang, J.; Robinson, P.T.; Xu, X.; Ba, D.; Li, Y.; Zhang, Z.; Rong, H. Diamonds and other exotic minerals recovered from peridotites of the Dangqiong Ophiolite, western Yarlung–Zangbo suture zone, Tibet. *Acta Geol. Sin.* **2016**, *90*, 425–439.
26. Xu, X.; Yang, J.; Robinson, P.T.; Xiong, F.; Ba, D.; Guo, G. Origin of ultrahigh pressure and highly reduced minerals in podiform chromitites and associated mantle peridotites of the Luobusa ophiolite, Tibet. *Gondwana Res.* **2015**, *27*, 686–700. [CrossRef]
27. Yang, J.S.; Meng, F.; Xu, S.; Robinson, P.T.; Dilek, Y.; Makeyev, A.B.; Wirth, R.; Wiedenbeck, M.; Cliff, J. Diamonds, native elements and metal alloys from chromitite of the Ray-Iz ophiolite of the Polar Urals. *Gondwana Res.* **2015**, *27*, 459–485. [CrossRef]
28. Farré de Pablo, J.; Proenza, J.; González-Jiménez, J.M.; Aiglsperger, T.; Garcia-Casco, A.; Escuder-Viruete, J.; Colás, V.; Longo, F. Ophiolite hosted chromitite formed by supra-subduction zone peridotite–plume interaction. *Geosci. Front.* **2020**. [CrossRef]
29. Pujol-Solà, N.; Proenza, J.A.; Garcia-Casco, A.; González-Jiménez, J.M.; Andreazini, A.; Melgarejo, J.C.; Gervilla, F. An alternative scenario on the origin of ultra-high pressure (UHP) and super-reduced (SUR) minerals in ophiolitic chromitites: A case study from the mercedita deposit (Eastern Cuba). *Minerals* **2018**, *8*, 433. [CrossRef]
30. Farré de Pablo, J.; Proenza, J.; González-Jiménez, J.M.; Garcia-Casco, A.; Colás, V.; Roqué-Rosell, J.; Camprubí, A.; Sánchez-Navas, A. A shallow origin for diamonds in ophiolitic chromitites. *Geology* **2018**, *47*, 75–78. [CrossRef]
31. Frei, R.; Gervilla, F.; Meibom, A.; Proenza, J.A.; Garrido, C.J. Os isotope heterogeneity of the upper mantle: Evidence from the Mayarí–Baracoa ophiolite belt in eastern Cuba. *Earth Planet. Sci. Lett.* **2006**, *241*, 466–476. [CrossRef]
32. Shi, R.; Alard, O.; Zhi, X.; O'Reilly, S.Y.; Pearson, N.J.; Griffin, W.L.; Zhang, M.; Chen, X. Multiple events in the Neo-Tethyan oceanic upper mantle: Evidence from Ru–Os–Ir alloys in the Luobusa and Dongqiao ophiolitic podiform chromitites, Tibet. *Earth Planet. Sci. Let.* **2007**, *261*, 33–48. [CrossRef]
33. Shi, R.; Griffin, W.L.; O'Reilly, S.; Huang, Q.; Zhang, X.; Liu, D.; Zhi, X.; Xia, Q.; Ding, L. Melt/mantle mixing produces podiform chromite deposits in ophiolites: Implications of Re–Os systematics in the Dongqiao Neo-tethyan ophiolite, northern Tibet. *Gondwana Res.* **2012**, *21*, 194–206. [CrossRef]
34. Malitch, K.N.; Junk, S.A.; Thalhammer, O.A.R.; Melcher, F.; Knauf, V.V.; Pernicka, E.; Stumpfl, E.F. Laurite and ruarsite from podiform chromitites at Kraubath and Hochgrössen, Austria: New insights from osmium isotopes. *Can. Mineral.* **2003**, *41*, 331–352. [CrossRef]
35. Malitch, K.N. Osmium isotope constraints on contrasting sources and prolonged melting in the Proterozoic upper mantle: Evidence from ophiolitic Ru–Os sulfides and Ru–Os–Ir alloys. *Chem. Geol.* **2004**, *208*, 157–173. [CrossRef]
36. Ahmed, A.H.; Hanghøj, K.; Kelemen, P.B.; Hart, S.R.; Arai, S. Osmium isotope systematics of the Proterozoic and Phanerozoic ophiolitic chromitites: In situ ion probe analysis of primary Os-rich PGM. *Earth Planet. Sci. Let.* **2006**, *245*, 777–791. [CrossRef]

37. Marchesi, C.; González-Jiménez, J.M.; Gervilla, F.; Garrido, C.J.; Griffin, W.L.; O'Reilly, S.Y.; Proenza, J.A.; Pearson, N.J. In situ Re–Os isotopic analysis of platinum-group minerals from the Mayarí–Cristal ophiolitic massif (Mayarí–Baracoa Ophiolitic Belt, eastern Cuba): Implications for the origin of Os-isotope heterogeneities in podiform chromitites. *Contrib. Mineral. Petrol.* **2011**, *161*, 977–990. [CrossRef]
38. González-Jiménez, J.M.; Griffin, W.L.; Gervilla, F.; Kerestedjian, T.; O'Reilly, S.Y.; Proenza, J.; Pearson, B.J.; Sergeeva, I. Metamorphism disturbs the Re-Os signatures of platinum-group minerals in ophiolite chromitites. *Geology* **2012**, *40*, 659–662. [CrossRef]
39. González-Jiménez, J.; Marchesi, C.; Griffin, W.L.; Gutiérrez-Narbona, R.; Lorand, J.-P.; O'Reilly, S.Y.; Garrido, C.J.; Gervilla, F.; Pearson, N.J.; Hidas, K. Transfer of Os isotopic signatures from peridotite to chromitite in the subcontinental mantle: Insights from in situ analysis of platinum-group and base-metal minerals (Ojén peridotite massif, southern Spain). *Lithos* **2013**, *164–167*, 74–85. [CrossRef]
40. González-Jiménez, J.M.; Locmelis, M.; Belousova, E.; Griffin, W.L.; Gervilla, F.; Kerestedjian, T.; O'Reilly, S.Y.; Sergeeva, I.; Pearson, N.J. Genesis and tectonic implications of podiform chromitites in the metamorphosed Ultramafic Massif of Dobromirtsi (Bulgaria). *Gond. Res.* **2015**, *27*, 555–574. [CrossRef]
41. Pearson, D.G.; Parman, S.W.; Nowell, G.M. A link between large mantle melting events and continent growth seen in osmium isotopes. *Nature* **2007**, *449*, 202–205. [CrossRef] [PubMed]
42. Xiong, Q.; Xu, Y.; González-Jiménez, J.M.; Liu, J.; Alard, O.; Zheng, J.-P.; Griffin, W.L.; O'Reilly, S.Y. Sulfide in dunite channels reflects long-distance reactive migration of mid-ocean-ridge melts from mantle source to crust: A Re-Os isotopic perspective. *Earth Planet. Sci. Lett.* **2020**, *531*, 115969. [CrossRef]
43. Ghosh, B.; Mukhopadhyay, S.; Morishita, T.; Tamura, A.; Arai, S.; Bandyopadhyay, D.; Chattopadhaya, S.; Ovung, T.N. Diversity and evolution of suboceanic mantle: Constraints from Neotethyan ophiolites at the eastern margin of the Indian plate. *J. Asian Earth Sci.* **2018**, *160*, 67–77. [CrossRef]
44. Ghosh, B.; Bandyopadhyay, D.; Morishita, T. Andaman–Nicobar ophiolites, India: Origin, evolution and emplacement. *Geol. Soc. Lond. Mem.* **2017**, *47*, 95–110. [CrossRef]
45. Bandyopadhyay, D.; Hinsbergen, D.; Plunder, A.; Bandopadhyay, P.; Advokaat, E.; Chattopadhaya, S.; Morishita, T.; Ghosh, B. Andaman Ophiolite: An Overview. In *The Andaman Islands and Adjoining Offshore: Geology, Tectonics and Palaeoclimate*; Springer: Berlin, Germany, 2020; pp. 1–17.
46. Saha, A.; Santosh, M.; Ganguly, S.; Manikyamba, C.; Ray, J.; Dutta, J. Geochemical cycling during subduction initiation: Evidence from serpentinized mantle wedge peridotite in the south Andaman ophiolite suite. *Geosci. Front.* **2018**, 1–21, in press. [CrossRef]
47. Pal, T.; Chakraborty, P.P.; Duttagupta, T.; Singh, C.D. Geodynamic evolution of an outer arc in convergent margin of active Burma–Java subduction complex, a document from Andaman islands, Bay of Bengal. *Geol. Mag.* **2003**, *140*, 289–307. [CrossRef]
48. Ghosh, B.; Pal, T.; Bhattacharya, A.; Das, D. Petrogenetic implications of ophiolitic chromite from Rutland Island, Andaman—A boninitic parentage in supra-subduction setting. *Mineral. Petrol.* **2009**, *96*, 59–70. [CrossRef]
49. Pal, T. Petrology and geochemistry of the Andaman ophiolite: Melt–rock interaction in a suprasubduction-zone setting. *J. Geol. Soc. Lond.* **2011**, *168*, 1031–1045. [CrossRef]
50. Pedersen, R.B.; Searle, M.P.; Carter, A.; Bandopadhyay, P.C. U–Pb zircon age of the Andaman ophiolite: Implications for the beginning of subduction beneath the Andaman–Sumatra arc. *J. Geol. Soc. Lond.* **2010**, *167*, 1105–1112. [CrossRef]
51. Sarma, S.; Jafri, S.H.; Fletcher, I.R.; McNaughton, N.J. 2010. Constraints on the tectonic setting of the Andaman ophiolites, Bay of Bengal, India, from SHRIMP U–Pb zircon geochronology and platiogranite. *J. Geol.* **2010**, *118*, 691–697. [CrossRef]
52. Plunder, A.; Bandyopadhyay, D.; Ganerød, M.; Advokaat, E.; Ghosh, B.; Bandopadhyay, P.; Hinsbergen, D. History of subduction polarity reversal during arc-continent collision: Constraints from the Andaman ophiolite and its metamorphic sole. *Tectonics* **2020**, *39*, e2019TC005762. [CrossRef]
53. Ghosh, B.; Morishita, T.; Bhatta, K. Significance of chromian spinels from the mantle sequence of the Andaman ophiolite, India: Paleogeodynamic implications. *Lithos* **2013**, *164–167*, 86–96. [CrossRef]
54. Bhattacharya, A.; Pal, T.; Ghosh, B. Characterization of the accreted ophiolite slices of Rutland island, Andaman sea: Evolution in a suprasubduction zone setting. *Ofioliti* **2013**, *38*, 121–142.
55. Ghosh, B.; Bhatta, K. Podiform chromitites in lherzolitic mantle rocks (Andaman ophiolite, India): The role of magma/rock interaction and parental melt composition. *Bull. Soc. Geol. Fr.* **2014**, *185*, 123–130. [CrossRef]

56. Pouchou, J.L.; Pichoir, F. A new model for quantitative X-ray microanalysis. Part 1. Applications to the analysis of homogeneous samples (English Edition). *Rech. Aerosp.* **1984**, *3*, 11–38.
57. Droop, G.T.R. A general equation for estimating Fe^{3+} concentrations in ferromagnesian silicates and oxides from microprobe analyses, using stoichiometric criteria. *Mineral. Mag.* **1987**, *51*, 431–435. [CrossRef]
58. Griffin, W.L.; Powell, W.J.; Pearson, N.J.; O'Reilly, S.Y. GLITTER: Data reduction software for laser ablation ICP-MS. In *Laser Ablation-ICP-MS in the Earth Sciences*; Sylvester, P., Ed.; Mineralogical Association of Canada: Quebec City, QC, Canada, 2008; pp. 204–207.
59. Norman, M.D.; Pearson, N.J.; Sharma, A.; Griffin, W.L. Quantitative analysis of trace elements in geological materials by laser ablation ICP-MS: Instrumental operating conditions and calibration values of NIST glasses. *Geostand. Newsl.* **1996**, *20*, 247–261. [CrossRef]
60. Gao, S.; Liu, X.; Yuan, H.; Hattendorf, B.; Günther, D.; Chen, L.; Hu, S. Determination of forty-two major and trace elements in USGS and NIST SRM glasses by Laser Ablation-Inductively Coupled Plasma-Mass Spectrometry. *Geostand. Geoanal. Res.* **2002**, *26*, 181–196. [CrossRef]
61. Maurel, C.; Maurel, P. Étude Expérimentale de la distribution de l'aluminium entre bain silicaté basique et spinelle chromifère. Implications pétrogénétiques: Teneur en chrome des spinelles. *Bull. Mineral.* **1982**, *105*, 197–202. [CrossRef]
62. Rollinson, H.R. The geochemistry of mantle chromitites from the northern part of the Oman ophiolite: Inferred parental melt compositions. *Contrib. Mineral. Petrol.* **2008**, *156*, 273–288. [CrossRef]
63. Dönmez, C.; Keskin, S.; Günay, K.; Çolakoğlu, A.O.; Çiftçi, Y.; Uysal, İ.; Türkel, A.; Yıldırım, N. Chromite and PGE geochemistry of the Elekdağ ophiolite (Kastamonu, Northern Turkey): Implications for deep magmatic processes in a supra-subduction zone setting. *Ore Geol. Rev.* **2014**, *57*, 216–228. [CrossRef]
64. Kamenetsky, V.S.; Crawford, A.J.; Meffre, S. Factors controlling chemistry of magmatic spinel: An empirical study of associated olivine, Cr-spinel and melt inclusions from primitive rocks. *J. Petrol.* **2001**, *42*, 655–671. [CrossRef]
65. Maurel, C. *Étude Expérimentale de L'équilibre Spinelle Chromifère-Liquide Silicaté Basique*; Société Française de Minéralogie et cristallographie Congrès "Les Spinelles": Paris, France, 1984.
66. Nowell, G.M.; Pearson, D.G.; Parman, S.W.; Luguet, A.; Hanski, E. Precise and accurate $^{186}Os/^{188}Os$ and $^{187}Os/^{188}Os$ measurements by multi-collector plasma ionisation mass spectrometry, Part II: Laser ablation and its application to single-grain Pt–Os and Re–Os geochronology. *Chem. Geol.* **2008**, *248*, 394–426. [CrossRef]
67. Shirey, S.B.; Walker, R.J. The Re–Os isotope system in cosmochemistry and high-temperature geochemistry. *Ann. Rev. Earth Planet. Sci. Lett.* **1998**, *26*, 423–500. [CrossRef]
68. Walker, R.J.; Horan, M.F.; Morgan, J.W.; Becker, H.; Grossman, J.N.; Rubin, A.E. Comparative ^{187}Re–^{187}Os systematics of chondrites: Implications regarding early solar system processes. *Geochim. Cosmochim. Acta* **2002**, *66*, 4187–4201. [CrossRef]
69. Sambridge, M.; Lambert, D.D. Propagating errors in decay equations: Examples from the Re–Os isotopic system. *Geochim. Cosmochim. Acta* **1997**, *61*, 3019–3024. [CrossRef]
70. Proenza, J.; Zaccarini, F.; Lewis, J.; Longo, F.; Garuti, G. Chromian spinel composition and the platinum-group minerals of the PGE-rich Loma Peguera chromitites, Loma Caribe peridotites, Dominican Republic. *Can. Mineral.* **2007**, *45*, 631–648. [CrossRef]
71. O'Driscoll, B.; González-Jiménez, J.M. Petrogenesis of the Platinum-Group Minerals. *Rev. Min. Geochem.* **2016**, *81*, 489–578. [CrossRef]
72. Pagé, P.; Barnes, S.-J. Using trace elements in chromites to constrain the origin of podiform chromitites in the Thetford Mines ophiolite, Québec, Canada. *Econ. Geol.* **2009**, *104*, 997–1018. [CrossRef]
73. González-Jiménez, J.M.; Proenza, J.A.; Gervilla, F.; Melgarejo, J.C.; Blanco-Moreno, J.A.; Ruiz-Sánchez, R.; Griffin, W.L. High-Cr and high-Al chromitites from the Sagua de Tánamo district, Mayarí–Cristal ophiolitic massif (eastern Cuba): Constraints on their origin from mineralogy and geochemistry of chromian spinel and platinum group elements. *Lithos* **2011**, *125*, 101–121. [CrossRef]
74. Leblanc, M. Chromitite and ultramafic rock compositional zoning through a paleotransform fault, Poum, New Caledonia. *Econ. Geol.* **1995**, *90*, 2028–2039. [CrossRef]
75. Merlini, A.; Grieco, G.; Ottolini, L.; Diella, V. Probe and SIMS investigation of clinopyroxene inclusions in chromites from the Troodos chromitites (Cyprus): Implications for dunite–chromitite genesis. *Ore Geol. Rev.* **2011**, *44*, 70–81. [CrossRef]

76. Karipi, S.; Tsikouras, T.; Hatzipaganagiotou, K. The petrogenesis and tectonic setting of ultramafic rocks from Iti and Kallidromon mountains, continental central Greece: Vestiges of the Pindos ocean. *Can. Mineral.* **2006**, *44*, 267–287. [CrossRef]
77. Karipi, S.; Tsikouras, T.; Hatzipaganagiotou, K.; Grammatikopoulos, T. Petrogenetic significance of spinel-group minerals from the ultramafic rocks of the Iti and Kallidromon ophiolites (Central Greece). *Lithos* **2007**, *99*, 136–149. [CrossRef]
78. Arai, S.; Yurimoto, H. Podiform chromitites of the Tari—Misaka ultramafic complex, Southwest Japan, as mantle-melt interaction products. *Econ. Geol.* **1994**, *89*, 1279–1288. [CrossRef]
79. Foustoukos, D.I.; Bizimis, M.; Frisby, C.; Shirey, S.B. Redox controls on Ni-Fe-PGE mineralization and Re/Os fractionation during serpentinization of abyssal peridotite. *Geochim. Cosmochim. Acta* **2015**, *150*, 11–25. [CrossRef]
80. Malitch, K.; Anikina, E.; Badanina, I.; Belousova, E.; Pushkarev, E.; Khiller, V. Chemical composition and osmium isotope systematics of primary and secondary platinum-group mineral assemblages from high-Mg chromitite of the Nurali lherzolite massif, South Urals, Russia. *Geol. Ore Depos.* **2016**, *58*, 1–19. [CrossRef]
81. Brandon, A.D.; Walker, R.J.; Morgan, J.W.; Norman, M.D.; Prichard, H.M. Coupled ^{186}Os and ^{187}Os evidence for core-mantle interaction. *Science* **1998**, *280*, 1570–1573. [CrossRef]
82. Brenan, J.M.; Andrews, D. High-temperature stability of Laurite and Ru–Os–Ir alloy and their role in PGE fractionation in mafic magmas. *Can. Mineral.* **2001**, *39*, 341–360. [CrossRef]
83. Bockrath, C.; Ballhaus, C.; Holzheid, A. Stabilities of laurite RuS_2 and monosulphide liquid solution at magmatic temperature. *Chem. Geol.* **2004**, *208*, 265–271. [CrossRef]
84. Fonseca, R.O.C.; Brückel, K.; Bragagni, A.; Leitzke, F.P.; Speelmanns, I.M.; Wainwright, A.N. Fractionation of Rhenium from Osmium during noble metal alloy formation in association with sulfides: Implications for the interpretation of model ages in alloy-bearing magmatic rocks. *Geochim. Cosmochim. Acta* **2017**, *216*, 184–200. [CrossRef]
85. Wainwright, A.N.; Luguet, A.; Schreiber, A.; Fonseca, R.O.C.; Nowell, G.M.; Lorand, J.-P.; Wirth, R.; Janney, P.E. Nanoscale variations in ^{187}Os isotopic composition and HSE systematics in a Bultfontein peridotite. *Earth Planet. Sci. Lett.* **2016**, *447*, 60–71. [CrossRef]
86. Coggon, J.A.; Nowell, G.M.; Pearson, D.G.; Parman, S.W. Application of the ^{190}Pt–^{186}Os isotope system to dating platinum mineralization and ophiolite formation: An example from the Meratus Mountains, Borneo. *Econ. Geol.* **2011**, *106*, 93–117. [CrossRef]
87. Wood, S.A. Thermodynamic calculations of the volatility of the platinum group elements (PGE): The PGE content of fluids at magmatic temperatures. *Geochim. Cosmochim. Acta* **1987**, *61*, 3041–3050. [CrossRef]
88. Fonseca, R.O.C.; Laurenz, V.; Mallmann, G.; Luguet, A.; Hoehne, N.; Jochum, K.P. New constrains on the genesis and long-term stability of Os-rich alloys in the Earth's mantle. *Geochim. Cosmochim. Acta* **2012**, *87*, 227–242. [CrossRef]
89. Barnes, S.J.; Pagé, P.; Prichard, H.M.; Zientek, M.L.; Fisher, P.C. Chalcophile and platinum-group element distribution in the ultramafic series of the Stillwater complex, Mt, USA—Implications for processes enriching chromite layers in Os, Ir, Ru, and Rh. *Mineral. Depos.* **2016**, *51*, 25–47. [CrossRef]
90. Lorand, J.P.; Alard, O.; Luguet, A. Platinum-group element micronuggets and refertilization process in Lherz orogenic peridotite (northeastern Pyrenees, France). *Earth Planet. Sci. Lett.* **2010**, *289*, 298–310. [CrossRef]
91. Griffin, W.L.; Graham, S.; O'Reilly, S.Y.; Pearson, N.J. Lithosphere evolution beneath the Kaapvaal Craton: Re–Os systematics of sulfides in mantle-derived peridotites. *Chem. Geol.* **2004**, *208*, 89–118. [CrossRef]
92. González-Jiménez, J.M.; Villaseca, C.; Griffin, W.L.; Belousova, E.; Konc, Z.; Ancochea, E.; O'Reilly, S.Y.; Pearson, N.; Garrido, C.J.; Gervilla, F. The architecture of the European-Mediterranean Lithosphere: A synthesis of the Re–Os evidence. *Geology* **2013**, *41*, 547–550. [CrossRef]
93. Wang, T. Tectonic Domains and Tectonic Units in Asian Continent (Chapter 2). In *The Tectonics and Metallogenesis of Asia*; Springer: Berlin, Germany, 2020. [CrossRef]
94. Jayananda, M.; Santosh, M.; Aadhiseshan, K.R. Formation of Archean (3600–2500 Ma) continental crust in the Dharwar Craton, southern India. *Earth Sci. Rev.* **2018**, *181*, 12–42.
95. Mukherjee, R.; Mondal, S.; Frei, R.; Rosing, M.; Waight, T.; Zhong, H.; Kumar, G.R. The 3.1 Ga Nuggihalli chromite deposits, Western Dharwar craton (India): Geochemical and isotopic constraints on mantle sources, crustal evolution and implications for supercontinent formation and ore mineralization. *Lithos* **2012**, *155*, 392–409. [CrossRef]

96. Ravikant, V.; Chandra-Pant, N. Precambian/Early Paleozoic orogenic rocks in the Himalaya-remmants of the leading edge of the Indian Plate. *Proc. Indian Natl. Sci. Acad.* **2020**, *86*, 167–173.
97. Srivastava, R.; Samal, A.K.; Ernst, R.E.; Söderlund, U.; Shankar, R. Spatial and temporal distribution of large igneous provinces in the Indian Shield—Highlights of recent investigations. *Proc. Indian Natl. Sci. Acad.* **2020**, *86*, 313–330. [CrossRef]
98. Goodwin, A.M. *Precambrian Geology, the Dynamic Evolution of the Continental Crust—Chapter 1*; Academic Press: Oxford, UK, 1991.
99. Harvey, J.; Gannoun, A.; Burton, K.W.; Rogers, N.W.; Alard, O.; Parkinson, I.J. Ancient melt extraction from the oceanic upper mantle revealed by Re–Os isotopes in abyssal peridotites from the Mid-Atlantic ridge. *Earth Planet. Sci. Lett.* **2006**, *244*, 606–621. [CrossRef]
100. Liu, C.-Z.; Snow, J.E.; Hellebrand, E.; Brügmann, G.; von der Handt, A.; Büchl, A.; Hofmann, A.W. Ancient, highly heterogeneous mantle beneath Gakkel ridge, Arctic Ocean. *Nature* **2008**, *452*, 311–316. [CrossRef] [PubMed]
101. O'Reilly, S.Y.; Zhang, M.; Griffin, W.L.; Begg, G.; Hronsky, J. Ultradeep continental roots and their oceanic remnants: A solution to the geochemical "mantle reservoir" problem? *Lithos* **2009**, *112*, 1043–1054. [CrossRef]
102. Acharyya, S.K. Tectonic evolution of Indo-Burma range with sepecial reference to Naga-Manipur Hills. *Mem. Geol. Soc. India* **2009**, *75*, 25–43.

© 2020 by the authors. Licensee MDPI, Basel, Switzerland. This article is an open access article distributed under the terms and conditions of the Creative Commons Attribution (CC BY) license (http://creativecommons.org/licenses/by/4.0/).